Topological insulator nanostructures

Seung Sae Hong, Desheng Kong, and Yi Cui

Electrons in topological insulators possess unique electronic band structures and spin properties, promising a novel route to engineer material properties for electronics and energy science. Enhancing the surface state signal in electron transport is critical for both fundamental study of the surface states and future applications. Nanostructures of topological insulators naturally have large surface-to-volume ratios, effectively increasing the surface transport compared to the bulk contribution. Moreover, the unique morphology of topological insulator nanostructures results in various quantum effects of electronic states, which can tailor the surface band via quantum confinement. Here we review recent progress in topological insulator nanostructures. Material design and electron transport of topological insulator nanostructures are introduced, with an emphasis on the unique properties of nanostructures. A few examples of applications and future perspective in using these nanostructures are also discussed.

Introduction

Topological insulators (TIs) are a class of materials where the bulk is a band insulator, but the surface possesses electronic states carrying electric current.[1,2] One unique characteristic of the surface bands is the spin-momentum locking property—electrons have a single spin state perpendicular to their moving direction (i.e., a helical spin state). This unique spin nature of the gapless surface states holds promise for new electronics applications (i.e., spintronics devices and quantum information processes), as well as for applications in energy conversion such as thermoelectrics. TI materials, mostly metal dichalcogenides with small bulk bandgaps, can be synthesized in various forms such as bulk crystals, thin films, and nanostructures. Bulk crystals of topological insulators were important material platforms in the early stage of TI studies—topological surface states can be easily probed using surface-sensitive techniques despite the coexisting background bulk electrons.[3–9] However, when it comes to electron transport essential for TI studies and applications, the dominance of bulk carriers over surface conduction becomes a significant challenge.[10–13] A tiny amount (<1%) of vacancies and anti-site defects in the crystals easily populate bulk carriers, thus masking the surface state effect in electronic transport. Therefore, the material dimensions matter in order to make use of the surface electrons' unique properties in the surface-dominant transport regime.

TI nanostructures have several unique advantages compared to their bulk counterpart. First, their large surface-to-volume ratio naturally reduces the bulk carrier contribution in the overall electron transport.[14,15] Second, field-effect gating in nanostructures allows modulation of the Fermi level in a single device.[16] Together with enhanced surface effects, the gating control in TI nanostructures can achieve TI surface state-dominated electron transport.[17] Third, the unique morphology of nanomaterials may enable the manipulation of 2D surface states at reduced dimensions.[18] An interesting example of this is a nanowire, where its cross-section perimeter gets smaller than the electron mean free path—unusual 1D states emerge, suggesting novel topological electronic states.[18] Last, TI heterostructures can be fabricated within single nanostructures, opening the opportunity for versatile band structure engineering of the surface states.

In this review, we describe synthesis methods of topological insulator nanostructures with an emphasis on the material design to overcome material challenges. A few examples of TI nanostructure transport are presented. Finally, we briefly discuss potential applications and future research directions of TI nanostructures.

Material design of TI nanostructures

The development of nanostructured topological insulator materials and electronic devices is very relevant to practical

Seung Sae Hong, Department of Applied Physics, Stanford University, USA; seungsae@stanford.edu
Desheng Kong, Department of Materials Science and Engineering, Stanford University, USA; desheng@stanford.edu
Yi Cui, Department of Materials Science and Engineering, Stanford Institute for Materials and Energy Sciences, SLAC National Accelerator Laboratory, USA; yicui@stanford.edu

applications (see the Introductory article). A major challenge to utilize the surface properties of these materials in charge transport processes is associated with the excessive bulk carriers arising from crystal defects[19–21] and environmental doping.[10,11,22–24] Compared with the bulk crystals, TI nanostructures are promising systems for investigating the surface states due to the large surface-to-volume ratio. The HgTe/CdTe quantum well is the first TI with a 2D form, with metallic edges wrapping around the quantum well.[25–27] The observation of the quantum spin Hall effect in this system demonstrated the feasibility of accessing the exotic properties of TIs in low-dimensional electronic devices.[27] Extensive research efforts have led to the extension of the concepts of 2D TIs into 3D TIs with metallic states on the crystal surface protected by time-reversal symmetry.[28–30] This largely expands the pool of TI materials. It is worth mentioning that non-trivial surface states, which are protected by crystal symmetry, have also recently been observed on the topological crystalline insulators (TCIs), $Pb_{1-x}Sn_xSe$, $Pb_{1-x}Sn_xTe$, and SnTe.[31–35]

The most widely studied TIs are the binary chalcogenides of Bi_2Se_3, Bi_2Te_3, and Sb_2Te_3,[4–6] which possess a single Dirac cone of the surface states residing in a relatively large bulk bandgap (~0.2 to 0.3 eV), compared to the early example of the HgTe/CdTe quantum well structure (10 meV).[27] These compounds share similar tetradymite-type structures that are formed by stacking covalently bonded molecular layers with weak van der Waals interactions. Their TI nature is further identified in their solid solution $Bi_{2-x}Sb_xTe_{3-y}Se_y$ for a wide range of compositions[12,13,16,36–39]—a layered crystalline system with tunable composition to optimize the properties (see **Figure 1**a).

As shown in Figure 1b, the weak interlayer coupling allows facile preparation of ultrathin flakes by mechanical exfoliation of bulk crystals using Scotch tape[40]—the technique widely adopted to produce graphene from graphite.[41] The process essentially offers convenient access to TI nanomaterials with excellent quality. We further demonstrated that the concept can be generalized to exfoliate Bi_2Se_3 nanostructures by using an atomic force microscopy tip.[42] Alternatively, the top-down exfoliation can also be performed through a solution process, which allows the preparation of large quantities of thin flakes from bulk crystals.[43]

Bottom-up synthesis is also routinely employed to prepare TI nanostructures with well-defined morphologies. Quasi-1D nanoribbons of Bi_2Se_3 are often prepared in a horizontal tube furnace by a gold nanoparticle-catalyzed vapor transport process, in which the gold nanoparticle promotes 1D growth via the vapor-liquid-solid process[14,15] (Figure 1c). Solution synthesis is also employed to grow 1D nanoribbons by using a solvothermal process.[44] Two-dimensional

TI nanoplates are typically produced by catalyst-free vapor transport (see Figure 1d) or solvothermal synthesis.[45,46] Two-dimensional nanostructures of TIs in the form of thin films are synthesized using van der Waals epitaxy (see Figure 1e). The technique is highly tolerant of large lattice mismatch, allowing the growth of high-quality films on different substrates with triangle/hexagonal lattices.[47–51] Nanostructures of non-layered crystals, on the other hand, are primarily obtained through bottom-up synthesis. For example, quasi-1D nanowires of SnTe, a TCI with a rock-salt structure, can be synthesized through a catalyst-free vapor transport process,[52] whereas their films are generated by molecular beam epitaxy.[53]

The presence of non-trivial surface states in solid solutions and doped crystals allows for the compositional engineering of TIs. Low-dimension nanostructures, with their large surface-to-volume ratios, provide excellent geometries to probe the surface states. A significant fraction of conductivity, however, still comes from bulk carriers in most non-doped nanomaterials. Accordingly, various dopants are frequently employed to reduce the number of bulk carriers through compensational doping. In addition, the alloying approach of parent compounds in the form of a solid solution, for example in $(Bi_xSb_{1-x})_2Te_3$, is also used to manipulate carrier type and density through compositional tuning (**Figure 2**a–c).[16,39] These efforts allow access to TIs with suppressed bulk conductivity, in which the charge transport is dominated by surface states.[16,17] The suppression of bulk carrier density is further confirmed by observing pronounced ambipolar field effects (see Figure 2d), in which the Fermi level is electrostatically manipulated with gate voltage.[16,17] The minimum carrier density of ~2×10^{11} cm^{-2} achieved in the Sb-doped

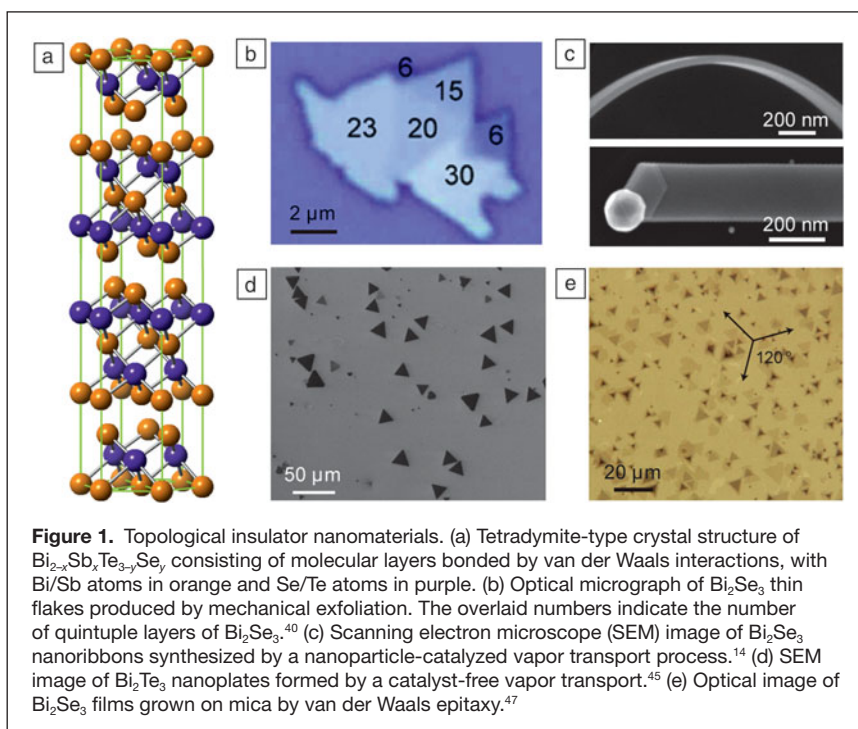**Figure 1.** Topological insulator nanomaterials. (a) Tetradymite-type crystal structure of $Bi_{2-x}Sb_xTe_{3-y}Se_y$ consisting of molecular layers bonded by van der Waals interactions, with Bi/Sb atoms in orange and Se/Te atoms in purple. (b) Optical micrograph of Bi_2Se_3 thin flakes produced by mechanical exfoliation. The overlaid numbers indicate the number of quintuple layers of Bi_2Se_3.[40] (c) Scanning electron microscope (SEM) image of Bi_2Se_3 nanoribbons synthesized by a nanoparticle-catalyzed vapor transport process.[14] (d) SEM image of Bi_2Te_3 nanoplates formed by a catalyst-free vapor transport.[45] (e) Optical image of Bi_2Se_3 films grown on mica by van der Waals epitaxy.[47]
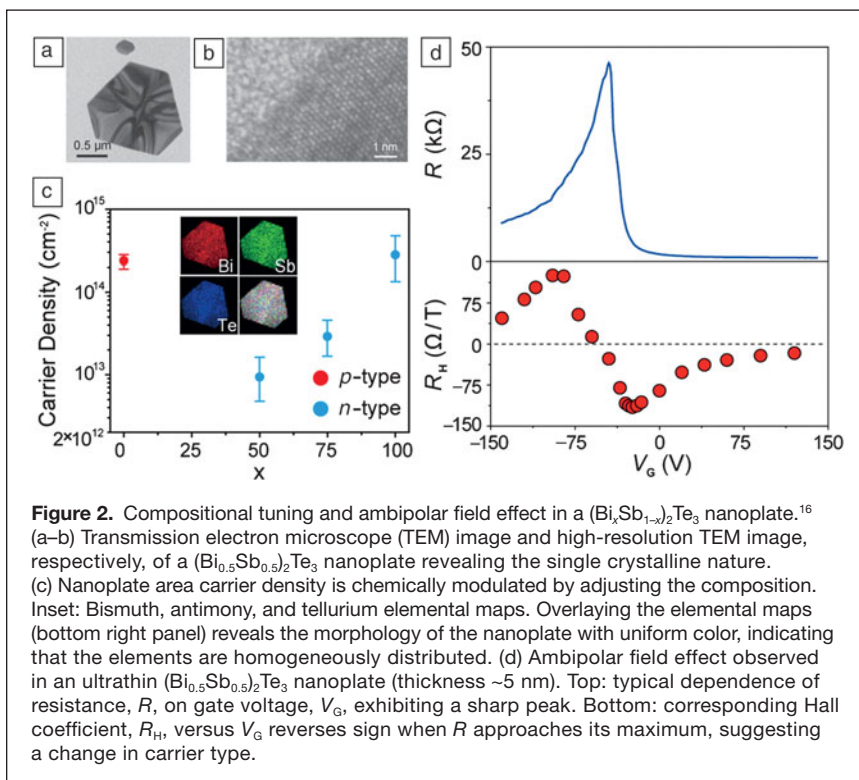
Figure 2. Compositional tuning and ambipolar field effect in a $(Bi_xSb_{1-x})_2Te_3$ nanoplate.[16] (a–b) Transmission electron microscope (TEM) image and high-resolution TEM image, respectively, of a $(Bi_{0.5}Sb_{0.5})_2Te_3$ nanoplate revealing the single crystalline nature. (c) Nanoplate area carrier density is chemically modulated by adjusting the composition. Inset: Bismuth, antimony, and tellurium elemental maps. Overlaying the elemental maps (bottom right panel) reveals the morphology of the nanoplate with uniform color, indicating that the elements are homogeneously distributed. (d) Ambipolar field effect observed in an ultrathin $(Bi_{0.5}Sb_{0.5})_2Te_3$ nanoplate (thickness ~5 nm). Top: typical dependence of resistance, R, on gate voltage, V_G, exhibiting a sharp peak. Bottom: corresponding Hall coefficient, R_H, versus V_G reverses sign when R approaches its maximum, suggesting a change in carrier type.

Bi_2Se_3 nanoribbon is much lower than for $(Bi_{0.5}Sb_{0.5})_2Te_3$, presumably due to the exposed Dirac point within the bulk bandgap accessible by gating.[17]

Electronic transport in topological insulator nanostructures

Enhanced surface electron contribution in TI nanostructures provides an ideal platform for probing electron transport of the topological surface states. We review a few examples of electronic transport studies of TI nanostructures. More specifically, Shubnikov-de Haas (SdH) oscillations (i.e., quantum oscillations in magneto-resistance observed at high magnetic field) from TI nanostructures have been reported, following the initial observations from TI bulk crystals.[11–13] The unique morphology and dimensions comparable to the phase coherence length/mean free path of the surface electrons have led to observations of quantum interference and 1D states. Finally, proximity-induced superconductivity (i.e., the superconducting transition of non-superconducting materials in contact with a superconductor) has also been observed in TI nanostructures.

Shubnikov-de Haas oscillations

The complexity of the band structures in topological insulator materials—surface bands, bulk bands, and impurity bands—makes it difficult to characterize the surface state via transport. SdH oscillations provide an effective tool to characterize a single band's parameters such as the size of the Fermi surface, effective electron mass, and band dispersion.

In TI nanostructures, a number of studies have reported SdH oscillations.[44,54–56] Gate-tunable SdH oscillations and 2D angle dependence of SdH oscillations have been reported, suggesting that high mobility carriers generating SdH oscillations are likely from the topological surface states. However, quantum-confined bulk-like carriers in very thin devices or the surface doped layers may behave in a similar manner, thus requiring careful studies to diagnosis the nature of the SdH oscillations.

Aharonov–Bohm effect and 1D topological states

The Aharonov-Bohm (AB) effect is a quantum phenomenon that originates from the electromagnetic potential difference between two separate electron paths, which results in a periodic modulation of the electron propagation probability by changing the magnetic field enclosed by the paths. Since the earliest demonstration of the AB effect in solid state systems—metallic ring structures, h/e or $h/2e$ periodicity in magnetoresistance has been understood as evidence of coherent electron transport (e.g., in carbon nanotubes [CNTs]).[57,58] In a topological insulator nanowire device exposed to a magnetic flux along the long axis, all surface electrons will gain identical phase from the magnetic flux Φ, while bulk carriers experiencing an external magnetic field would generate no regular periodicity. The first AB oscillations in topological insulator nanowires were reported in Bi_2Se_3 nanowires,[14] providing strong evidence of topological surface electron conduction in a coherent manner (**Figure 3**). Subsequently, many other nanowires of candidate topological insulators also manifest AB oscillations, for example, Bi_2Te_3, β–Ag_2Te, and SnTe nanowires.[44,52,59]
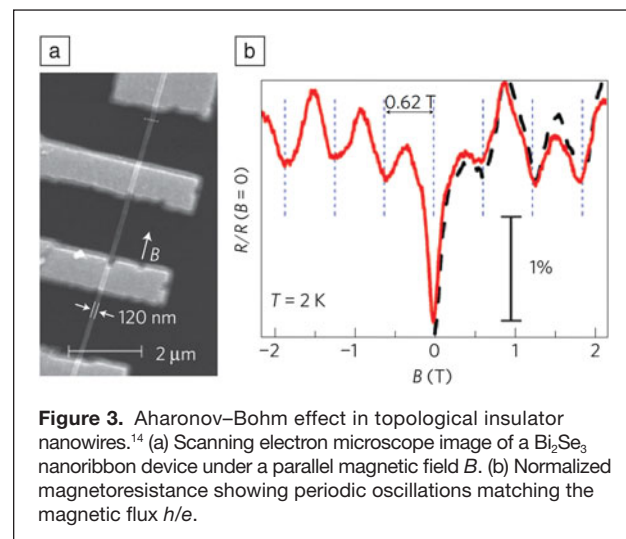

Figure 3. Aharonov–Bohm effect in topological insulator nanowires.[14] (a) Scanning electron microscope image of a Bi_2Se_3 nanoribbon device under a parallel magnetic field B. (b) Normalized magnetoresistance showing periodic oscillations matching the magnetic flux h/e.
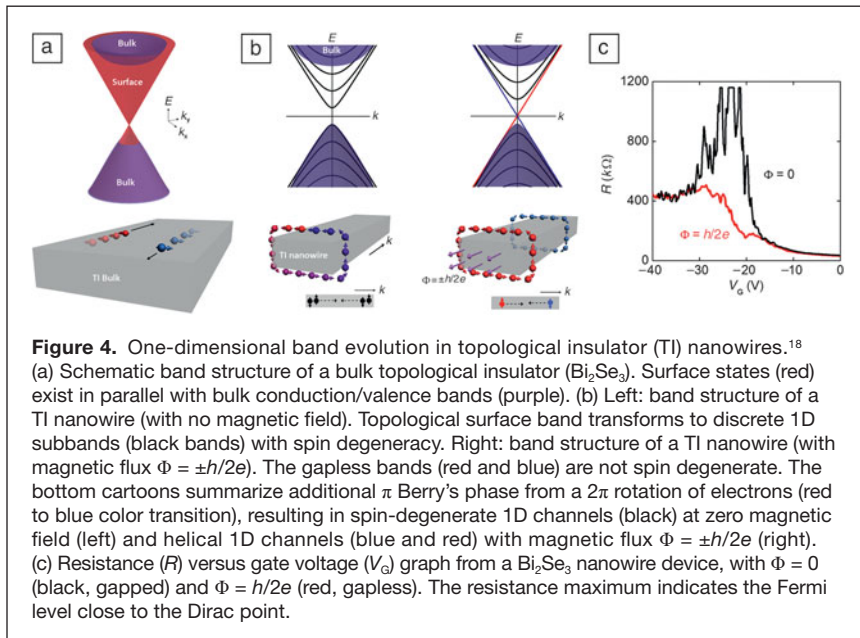
Figure 4. One-dimensional band evolution in topological insulator (TI) nanowires.[18] (a) Schematic band structure of a bulk topological insulator (Bi_2Se_3). Surface states (red) exist in parallel with bulk conduction/valence bands (purple). (b) Left: band structure of a TI nanowire (with no magnetic field). Topological surface band transforms to discrete 1D subbands (black bands) with spin degeneracy. Right: band structure of a TI nanowire (with magnetic flux $\Phi = \pm h/2e$). The gapless bands (red and blue) are not spin degenerate. The bottom cartoons summarize additional π Berry's phase from a 2π rotation of electrons (red to blue color transition), resulting in spin-degenerate 1D channels (black) at zero magnetic field (left) and helical 1D channels (blue and red) with magnetic flux $\Phi = \pm h/2e$ (right). (c) Resistance (R) versus gate voltage (V_G) graph from a Bi_2Se_3 nanowire device, with $\Phi = 0$ (black, gapped) and $\Phi = h/2e$ (red, gapless). The resistance maximum indicates the Fermi level close to the Dirac point.

In addition, AB oscillations in TI nanowires suggest a different type of electronic band structure made of the surface electrons—1D states of the topological surface states.[60,61] When the surface electrons' mean free path exceeds the circumference of the nanowire cross-section, momentum quantization brings one-dimensional subband formation out of 2D surface electrons. Interestingly, these 1D subbands can be periodically modulated by a magnetic flux, giving magneto-oscillations in conductance (**Figure 4**a–b). Unlike the 1D subband formation in the "graphene to CNT transition," the surface electrons on TI nanowires have an additional phase factor (π) from the spin-momentum interlocking nature, which is known as the spin Berry phase (spins of the surface electrons make a 2π rotation along the nanowire circumference and acquire π phase due to electrons' fermionic nature, spin = 1/2). Thus, all the 1D subbands of surface electrons are gapped at zero magnetic field. However, the magnetic half quantum flux ($\Phi = h/2e$) restores a gapless 1D mode. A recent experiment by Hong et al. indeed showed such a gap closing transition tuned by a magnetic field (Figure 4c).[18] A more detailed study of the gapless state at $\Phi = h/2e$ revealed that it is robust against additional impurities, strong enough to suppress most quantum interferences, but it can be easily destroyed under time-reversal symmetry breaking (i.e., perpendicular magnetic field).

Superconducting proximity effect

Proximity-induced superconductivity in TI nanostructures is one of the most intensely studied topics in TI electron transport, as the interface between a TI and a conventional superconductor (SC) can generate many exotic phenomena such as a Majorana fermion, a quasi-particle excitation that becomes its own anti-particle.[62–64] The Majorana fermion is interesting not only in the context of fundamental scientific interest, but also in novel electronic applications of quantum information processing. Nanodevices made of TI nanomaterials can easily accommodate proximity-induced superconductivity by depositing superconducting metallic electrodes. Several groups have reported the superconducting proximity effect in TI nanostructures[54,65–67] and have confirmed that the supercurrent is carried via surface states.[66] The configuration of TI Josephson junctions, SC-TI-SC junctions where two SC materials are weakly linked via a TI material, are used to probe Majorana fermions in the superconducting TI devices.[67] Despite many experimental challenges, continuous progress in TI superconductivity suggest novel device realization in the coming years.

Applications and future perspective

Spin-textured surface states are attractive for novel electronics. The spin-momentum locking nature of the surface electrons suggests an electrical manipulation of spin currents, which is naturally desirable for spintronics applications. One of the practical challenges is spin injection from ferromagnetic contact to TI materials, requiring further experimental efforts in interface engineering. TI materials (i.e., Bi_2Te_3) are also well known for their superior thermoelectric properties.[68] The thermoelectric figure of merit is expected to be improved by making use of surface states decoupling with electronic heat conduction. In particular, TI nanowires and nanoplates are ideal material forms for thermal transport measurements in suspended geometries (**Figure 5**a) and are expected to enhance thermoelectric performance.[69,70]

The layered structure of Bi_2Se_3, Bi_2Te_3, and their alloys imply that TI nanostructures can be broadly defined as 2D materials. Combined with many other 2D atomic crystals,
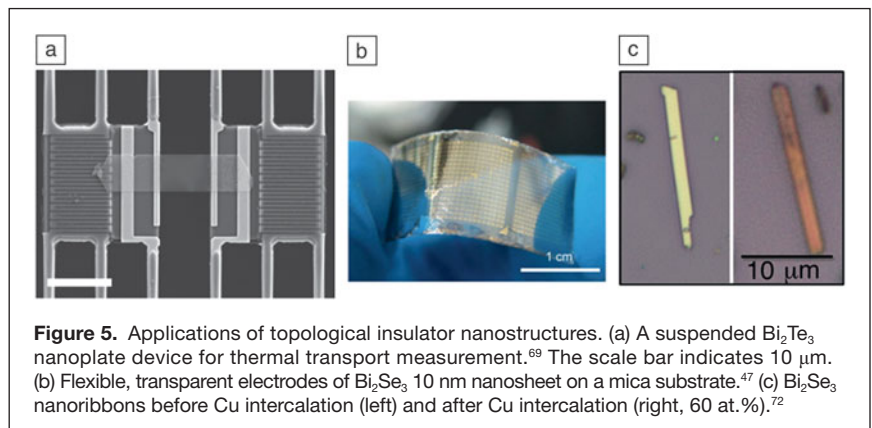

Figure 5. Applications of topological insulator nanostructures. (a) A suspended Bi_2Te_3 nanoplate device for thermal transport measurement.[69] The scale bar indicates 10 μm. (b) Flexible, transparent electrodes of Bi_2Se_3 10 nm nanosheet on a mica substrate.[47] (c) Bi_2Se_3 nanoribbons before Cu intercalation (left) and after Cu intercalation (right, 60 at.%).[72]

TI nanostructures provide building blocks for 2D van der Waals heterostructures[71] with unique electronic states. A few examples of transparent electrodes demonstrate how TI nanomaterials can be used for applications like many other 2D layered materials (Figure 5b). For example, the surface states in Bi_2Se_3 will enhance the electrical conductivity of the electrode material, while the thin film of Bi_2Se_3 maintains high optical transmittance over a wide range of wavelengths.[47] The layered structure with van der Waals gaps is an interesting playground for intercalation. Chemical intercalation of metal atoms and organic molecules into TI nanomaterials has been reported;[72–74] some metal atoms/ions (i.e., zero-valence copper) can be intercalated up to 60% in atomic percentage, modifying electronic and optical properties (Figure 5c). The chemistry and electrochemistry of TI nanomaterials has not been fully developed yet, but more in-depth studies are expected in the future.

Here, we briefly reviewed the progress in TI nanostructures over the last few years. Despite their short history, TI nanostructures have provided many intriguing examples of both fundamental studies and applications. As more device applications of TIs develop, TI nanostructures will gain more interest. This field is fertile ground for both physics and applications for years to come.

Acknowledgments

References

1. M.Z. Hasan, C.L. Kane, *Rev. Mod. Phys.* **82**, 3045 (2010).
2. X.-L. Qi, S.-C. Zhang, *Rev. Mod. Phys.* **83**, 1057 (2011).
3. D. Hsieh, D. Qian, L. Wray, Y. Xia, Y.S. Hor, R.J. Cava, M.Z. Hasan, *Nature* **452**, 970 (2008).
4. H. Zhang, C.X. Liu, X.L. Qi, X. Dai, Z. Fang, S.C. Zhang, *Nat. Phys.* **5**, 438 (2009).
5. Y. Xia, D. Qian, D. Hsieh, L. Wray, A. Pal, H. Lin, A. Bansil, D. Grauer, Y.S. Hor, R.J. Cava, M.Z. Hasan, *Nat. Phys.* **5**, 398 (2009).
6. Y. Chen, J.G. Analytis, J.-H. Chu, Z.K. Liu, S.-K. Mo, X.L. Qi, H.J. Zhang, D.H. Lu, X. Dai, Z. Fang, S.C. Zhang, I.R. Fisher, Z. Hussain, Z.-X. Shen, *Science* **325**, 178 (2009).
7. P. Roushan, J. Seo, C.V. Parker, Y.S. Hor, D. Hsieh, D. Qian, A. Richardella, M.Z. Hasan, R.J. Cava, A. Yazdani, *Nature* **460**, 1106 (2009).
8. T. Zhang, P. Cheng, X. Chen, J.F. Jia, X. Ma, K. He, L. Wang, H. Zhang, X. Dai, Z. Fang, X. Xie, Q.K. Xue, *Phys. Rev. Lett.* **103**, 266803 (2009).
9. T. Hanaguri, K. Igarashi, M. Kawamura, H. Takagi, T. Sasagawa, *Phys. Rev. B: Condens. Matter* **82**, 081305 (2010).
10. J.G. Analytis, J.-H. Chu, Y. Chen, F. Corredor, R.D. McDonald, Z.X. Shen, I.R. Fisher, *Phys. Rev. B: Condens. Matter* **81**, 205407 (2010).
11. J.G. Analytis, R.D. McDonald, S.C. Riggs, J.-H. Chu, G.S. Boebinger, I.R. Fisher, *Nat. Phys.* **6**, 960 (2010).
12. J. Xiong, A.C. Petersen, D. Qu, Y.S. Hor, R.J. Cava, N.P. Ong, *Physica E* **44**, 917 (2012).
13. Z. Ren, A.A. Taskin, S. Sasaki, K. Segawa, Y. Ando, *Phys. Rev. B: Condens. Matter* **82**, 241306 (2010).
14. H. Peng, K. Lai, D. Kong, S. Meister, Y. Chen, X.L. Qi, S.C. Zhang, Z.X. Shen, Y. Cui, *Nat. Mater.* **9**, 225 (2010).
15. D. Kong, J.C. Randel, H. Peng, J.J. Cha, S. Meister, K. Lai, Y. Chen, Z.-X. Shen, H.C. Manoharan, Y. Cui, *Nano Lett.* **10** 329 (2010).
16. D. Kong, Y. Chen, J.J. Cha, Q. Zhang, J.G. Analytis, K. Lai, Z. Liu, S.S. Hong, K.J. Koski, S.-K. Mo, Z. Hussain, I.R. Fisher, Z.-X. Shen, Y. Cui, *Nat. Nanotechnol.* **6**, 705 (2011).
17. S.S. Hong, J.J. Cha, D. Kong, Y. Cui, *Nat. Commun.* **3**, 757 (2012).
18. S.S. Hong, Y. Zhang, J.J. Cha, X.L. Qi, Y. Cui, *Nano Lett.* **14**, 2815 (2014).
19. J. Navrátil, J. Horák, T. Plecháček, S. Kamba, P. Lošťák, J.S. Dyck, W. Chen, C. Uher, *J. Solid State Chem.* **177**, 1704 (2004).
20. G. Wang, X.-G. Zhu, Y.-Y. Sun, Y.-Y. Li, T. Zhang, J. Wen, X. Chen, K. He, L.-L. Wang, X.-C. Ma, J.-F. Jia, S.B. Zhang, Q.-K. Xue, *Adv. Mater.* **23**, 2929 (2011).
21. Y. Jiang, Y.Y. Sun, M. Chen, Y. Wang, Z. Li, C. Song, K. He, L. Wang, X. Chen, Q.-K. Xue, X. Ma, S.B. Zhang, *Phys. Rev. Lett.* **108**, 066809 (2012).
22. D. Kong, J.J. Cha, K. Lai, H. Peng, J.G. Analytis, S. Meister, Y. Chen, H.-J. Zhang, I.R. Fisher, Z.-X. Shen, Y. Cui, *ACS Nano* **5**, 4698 (2011).
23. H.M. Benia, C. Lin, K. Kern, C.R. Ast, *Phys. Rev. Lett.* **107**, 177602 (2011).
24. C. Chen, S. He, H. Weng, W. Zhang, L. Zhao, H. Liu, X. Jia, D. Mou, S. Liu, J. He, Y. Peng, Y. Feng, Z. Xie, G. Liu, X. Dong, J. Zhang, X. Wang, Q. Peng, Z. Wang, S. Zhang, F. Yang, C. Chen, Z. Xu, X. Dai, Z. Fang, X.J. Zhou, *Proc. Natl. Acad. Sci. U.S.A.* (2012), doi:10.1073/pnas.1115555109.
25. C.L. Kane, E.J. Mele, *Phys. Rev. Lett.* **95**, 146802 (2005).
26. B.A. Bernevig, T.L. Hughes, S.-C. Zhang, *Science* **314**, 1757 (2006).
27. M. König, S. Wiedmann, C. Brüne, A. Roth, H. Buhmann, L.W. Molenkamp, X.-L. Qi, S.-C. Zhang, *Science* **318**, 766 (2007).
28. L. Fu, C.L. Kane, E.J. Mele, *Phys. Rev. Lett.* **98**, 106803 (2007).
29. J.E. Moore, L. Balents, *Phys. Rev. B: Condens. Matter* **75**, 121306 (2007).
30. R. Roy, *Phys. Rev. B: Condens. Matter* **79**, 195321 (2009).
31. L. Fu, *Phys. Rev. Lett.* **106**, 106802 (2011).
32. P. Dziawa, B.J. Kowalski, K. Dybko, R. Buczko, A. Szczerbakow, M. Szot, E. Łusakowska, T. Balasubramanian, B.M. Wojek, M.H. Berntsen, O. Tjernberg, T. Story, *Nat. Mater.* **11**, 1023 (2012).
33. S.-Y. Xu, C. Liu, N. Alidoust, M. Neupane, D. Qian, I. Belopolski, J.D. Denlinger, Y.J. Wang, H. Lin, L.A. Wray, G. Landolt, B. Slomski, J.H. Dil, A. Marcinkova, E. Morosan, Q. Gibson, R. Sankar, F.C. Chou, R.J. Cava, A. Bansil, M.Z. Hasan, *Nat. Commun.* **3**, 1192 (2012).
34. Y. Tanaka, Z. Ren, T. Sato, K. Nakayama, S. Souma, T. Takahashi, K. Segawa, Y. Ando, *Nat. Phys.* **8**, 800 (2012).
35. T.H. Hsieh, H. Lin, J. Liu, W. Duan, A. Bansil, L. Fu, *Nat. Commun.* **3**, 982 (2012).
36. Z. Ren, A.A. Taskin, S. Sasaki, K. Segawa, Y. Ando, *Phys. Rev. B: Condens. Matter* **84**, 165311 (2011).
37. T. Arakane, T. Sato, S. Souma, K. Kosaka, K. Nakayama, M. Komatsu, T. Takahashi, Z. Ren, K. Segawa, Y. Ando, *Nat. Commun.* **3**, 636 (2012).
38. J.J. Cha, D. Kong, S.S. Hong, J.G. Analytis, K. Lai, Y. Cui, *Nano Lett.* **12**, 1107 (2012).
39. J. Zhang, C.-Z. Chang, Z. Zhang, J. Wen, X. Feng, K. Li, M. Liu, K. He, L. Wang, X. Chen, Q.-K. Xue, X. Ma, Y. Wang, *Nat. Commun.* **2**, 574 (2011).
40. J.G. Checkelsky, Y.S. Hor, R.J. Cava, N.P. Ong, *Phys. Rev. Lett.* **106**, 196801 (2011).
41. K.S. Novoselov, A.K. Geim, S.V. Morozov, D. Jiang, Y. Zhang, S.V. Dubonos, I.V. Grigorieva, A.A. Firsov, *Science* **306**, 666 (2004).
42. S.S. Hong, W. Kundhikanjana, J.J. Cha, K. Lai, D. Kong, S. Meister, M.A. Kelly, Z.-X. Shen, Y. Cui, *Nano Lett.* **10**, 3118 (2010).
43. J.N. Coleman, M. Lotya, A. O'Neill, S.D. Bergin, P.J. King, U. Khan, K. Young, A. Gaucher, S. De, R.J. Smith, I.V. Shvets, S.K. Arora, G. Stanton, H.-Y. Kim, K. Lee, G.T. Kim, G.S. Duesberg, T. Hallam, J.J. Boland, J.J. Wang, J.F. Donegan, J.C. Grunlan, G. Moriarty, A. Shmeliov, R.J. Nicholls, J.M. Perkins, E.M. Grieveson, K. Theuwissen, D.W. McComb, P.D. Nellist, V. Nicolosi, *Science* **331**, 568 (2011).
44. F. Xiu, L. He, Y. Wang, L. Cheng, L.-T. Chang, M. Lang, G. Huang, X. Kou, Y. Zhou, X. Jiang, Z. Chen, J. Zou, A. Shailos, K. Wang, *Nat. Nanotechnol.* **6**, 216 (2011).
45. D. Kong, W. Dang, J.J. Cha, H. Li, S. Meister, H. Peng, Z. Liu, Y. Cui, *Nano Lett.* **10**, 2245 (2010).
46. D. Kong, K.J. Koski, J.J. Cha, S.S. Hong, Y. Cui, *Nano Lett.* **13**, 632 (2013).
47. H. Peng, W. Dang, J. Cao, Y. Chen, D. Wu, W. Zheng, H. Li, Z.-X. Shen, Z. Liu, *Nat. Chem.* **4**, 281 (2012).
48. X. Chen, X.-C. Ma, K. He, J.-F. Jia, Q.-K. Xue, *Adv. Mater.* **23**, 1162 (2011).
49. A.A. Taskin, S. Sasaki, K. Segawa, Y. Ando, *Phys. Rev. Lett.* **109**, 066803 (2012).
50. W. Dang, H. Peng, H. Li, P. Wang, Z. Liu, *Nano Lett.* **10**, 2870 (2010).
51. X.F. Kou, L. He, F.X. Xiu, M.R. Lang, Z.M. Liao, Y. Wang, A.V. Fedorov, X.X. Yu, J.S. Tang, G. Huang, X.W. Jiang, J.F. Zhu, J. Zou, K. Wang, *Appl. Phys. Lett.* **98**, 242102 (2011).
52. M. Safdar, Q. Wang, M. Mirza, Z. Wang, K. Xu, J. He, *Nano Lett.* **13**, 5344 (2013).
53. B.A. Assaf, F. Katmis, P. Wei, B. Satpati, Z. Zhang, S.P. Bennett, V.G. Harris, J.S. Moodera, D. Heiman, in press (2014), http://arxiv.org/abs/1403.1810.
54. B. Sacepe, J.B. Oostinga, J. Li, A. Ubaldini, N.J. Couto, E. Giannini, A.F. Morpurgo, *Nat. Commun.* **2**, 575 (2011).
55. L. Fang, Y. Jia, D.J. Miller, M.L. Latimer, Z.L. Xiao, U. Welp, G.W. Crabtree, W.K. Kwok, *Nano Lett.* **12**, 6164 (2012).
56. P. Gehring, B.F. Gao, M. Burghard, K. Kern, *Nano Lett.* **12**, 5137 (2012).
57. R.A. Webb, S. Washburn, C.P. Umbach, R.B. Laibowitz, *Phys. Rev. Lett.* **54**, 2696 (1985).

58. A. Bachtold, C. Strunk, J.P. Salvetat, J.M. Bonard, L. Forro, T. Nussbaumer, C. Schonenberger, *Nature* **397**, 673 (1999).

59. S. Lee, J. In, Y. Yoo, Y. Jo, Y.C. Park, H.-J. Kim, H.C. Koo, J. Kim, B. Kim, K.L. Wang, *Nano Lett.* **12**, 4194 (2012).

60. J.H. Bardarson, P.W. Brouwer, J.E. Moore, *Phys. Rev. Lett.* **105**, 156803 (2010).

61. Y. Zhang, A. Vishwanath, *Phys. Rev. Lett.* **105**, 206601 (2010).

62. A.Y. Kitaev, *Phys. Usp.* **44**, 131 (2001).

63. L. Fu, C.L. Kane, *Phys. Rev. Lett.* **100**, 096407 (2008).

64. J. Alicea, *Rep. Prog. Phys.* **75**, 076501 (2012).

65. D. Zhang, J. Wang, A.M. DaSilva, J.S. Lee, H.R. Gutierrez, M.H.W. Chan, J. Jain, N. Samarth, *Phys. Rev. B: Condens. Matter* **84**, 165120 (2011).

66. M. Veldhorst, M. Snelder, M. Hoek, T. Gang, V.K. Guduru, X.L. Wang, U. Zeitler, W.G. van der Wiel, A.A. Golubov, H. Hilgenkamp, A. Brinkman, *Nat. Mater.* **11**, 417 (2012).

67. J.R. Williams, A.J. Bestwick, P. Gallagher, S.S. Hong, Y. Cui, A.S. Bleich, J.G. Analytis, I.R. Fisher, D. Goldhaber-Gordon, *Phys. Rev. Lett.* **109**, 056803 (2012).

68. Y.S. Hor, A. Richardella, P. Roushan, Y. Xia, J.G. Checkelsky, A. Yazdani, M.Z. Hasan, N.P. Ong, R.J. Cava, *Phys. Rev. B: Condens. Matter* **79**, 195208 (2009).

69. M.T. Pettes, J. Maassen, I. Jo, M.S. Lundstrom, L. Shi, *Nano Lett.* **13**, 5316 (2013).

70. Y. Xu, Z. Gan, S.-C. Zhang (2014) (forthcoming), arXiv:1403.3137.

71. A.K. Geim, I.V. Grigorieva, *Nature* **499**, 419 (2013).

72. K.J. Koski, J.J. Cha, B.W. Reed, C.D. Wessells, D. Kong, Y. Cui, *JACS* **134**, 7584 (2012).

73. K.J. Koski, C.D. Wessells, B.W. Reed, J.J. Cha, D. Kong, Y. Cui, *JACS* **134**, 13773 (2012).

74. J.J. Cha, K.J. Koski, K.C.Y. Huang, K.X. Wang, W. Luo, D. Kong, Z. Yu, S. Fan, M.L. Brongersma, Y. Cui, *Nano Lett.* **13**, 5913 (2013). □